J Mater Sci (2010) 45:2816–2821
DOI 10.1007/s10853-010-4272-3

Fabrication of Al/TiB_2 composites through gas pressure infiltration

J. M. Molina · J. Tian · J. Narciso · E. Louis

Received: 7 July 2009 / Accepted: 25 January 2010 / Published online: 17 February 2010

Abstract Titanium diboride is being evaluated as a replacement of SiC in metal/ceramic composites for thermal management. Albeit these composites are produced by gas pressure infiltration, no study of the process is available. This work presents an analysis of the threshold pressure for infiltration of Al into TiB_2 compacts and of the infiltration kinetics. Particles of diameters 14 and 20 μm, and spans of 1.62 and 1.77, were packed obtaining a volume fraction of 0.63. The compacts were infiltrated in air with pure Al at 700 °C. Despite of the fact that the average particle radii differ in a 50%, the threshold pressure for the coarser particles is only a 4% lower, while intrinsic compact permeabilities (derived from infiltration of a wetting organic liquid) are identical. The origin of this apparently odd behavior is the almost identical specific surface areas that those two particles have. Contact angles derived from infiltration experiments are shown to be compatible with sessile drop results.

J. M. Molina (✉) · J. Tian · J. Narciso · E. Louis
Instituto Universitario de Materiales de Alicante, Universidad de Alicante, Apdo 99, 03080 Alicante, Spain
e-mail: jmmj@ua.es

J. M. Molina · E. Louis
Departamento de Física Aplicada, Universidad de Alicante, Apdo 99, 03080 Alicante, Spain

J. M. Molina · J. Tian · J. Narciso
Departamento de Química Inorgánica, Universidad de Alicante, Apdo 99, 03080 Alicante, Spain

J. Tian
Institute of Material Science and Engineering, Ocean University of China, 266100 Qingdao, People's Republic of China

E. Louis
Unidad Asociada del Consejo Superior de Investigaciones Científicas, Universidad de Alicante, Apdo 99, 03080 Alicante, Spain

Introduction

Titanium diboride is one of the ceramic compounds that are being evaluated as possible replacements of the highly successful SiC in metal/ceramic composites for thermal management [1]. TiB_2 has a reasonably high electrical conductivity (about 10^5 Siemens/cm) and a thermal conductivity of around 100 W/(m K) [2]. The fact that its thermal conductivity is substantially lower than that of SiC is, however, partially compensated by the much higher interfacial conductivity (it should be noted that while in SiC heat conduction is mainly mediated by phonons, in TiB_2 electrons are the main carriers, as in the host metal) [3]. Another feature of TiB_2 that makes it a serious candidate for these applications is that unlike ceramics with purely covalent nature, the thermal conductivity variation with temperature until 500 °C is rather negligible [2, 4].

Albeit the metal/TiB_2 composites are commonly produced by gas pressure infiltration, no detailed study of the process has yet been published. This work is addressed to fill up that gap, presenting a thorough analysis of the threshold pressure for infiltration of molten Al into TiB_2 particle compacts and of the infiltration kinetics. To this end two particles of average diameters 14 and 20 μm, and a similar span around 1.7 were packed into quartz tubes attaining a volume fraction of 0.63. The compacts were gas pressure infiltrated in air with pure Al at 700 °C. In addition, and in order to determine the intrinsic permeability of the compacts, a wetting organic fluid was infiltrated at room temperature. The results indicate that, despite of the fact that the average particle radii differ in no more than a

50%, the threshold pressure for the coarser particles is only a 2% lower. In addition, the intrinsic compact permeabilities are identical. The origin of this apparently odd behavior is the almost identical specific surface areas that those two particles have [5–8]. Contact angles derived from the infiltration experiments are shown to be compatible with sessile drop results.

Materials and experimental procedures

Materials

Commercially pure aluminum (purity ~99.98 wt%) and two kinds of TiB_2 ceramic particles, hereafter referred to as TiB_2(S) and TiB_2(C), were used in the present study. Their chemical compositions are reported in Table 1. The as-received particles were cleaned in a stirred ethanol bath for at least 3 times. After cleaning, the particles were dried at 110 °C for 2 h. Particle properties relevant to the present work are reported in Table 2. The size distribution and mean diameter were measured by means of Laser Scattering (LS), while the specific surface area was determined by means of the Brunauer, Emmett, and Teller (BET) technique. In addition, particle morphology was examined using scanning electron microscopy (SEM).

Particle surface chemistry

XPS spectra from the particles surface have been obtained with a VG-Microtech Multilab electron spectrometer, by using the Mg Kα (1253.6 eV) radiation of twin anode in the constant analyzer energy mode with pass energy of 50 eV.

Table 1 Chemical composition of the two TiB_2 particles used in this work

Particles	Ti	B	C	B_2O_3	O	N	Fe
TiB_2(S)	66.5	30.0	0.7	0.5	0.5	0.5	0.2
TiB_2(C)	66.0	30.0	2.0	2.5	0.5	0.5	0.2

The data are from the manufacturer and are reported in wt%

Table 2 Main properties of the two TiB_2 particles used in this work

Particles	ρ	D(4,3)	D(3,2)	D(10)	Span	S_{BET}	S_L	V_p
TiB_2(S)	4.51	13.7	8.2	4.5	1.62	350	162	0.63
TiB_2(C)	4.52	20.4	10.7	5.6	1.77	350	124	0.63

The Table reports data for: the average diameter D (D(4,3) and D(3,2) in μm), the span of the particle size distribution, defined as $[D(90) - D(10)]/D(50)$, where $D(x)$ is the diameter (also in μm) below which x% of the particles are found, the specific surface area of the particles S_L and S_{BET} (in m^2/kg) as measured by means of the laser scattering and BET technique, respectively, the density ρ in g/cm^3, and the average particle volume fraction V_p of the TiB_2 particle compacts

Pressure of the analysis chamber was maintained at 5×10^{-10} mbar. The binding energy and the Auger kinetic energy scale were calibrated by setting the C1s transition at 284.6 eV. The accuracy of BE and KE values was ±0.2 and ±0.3 eV, respectively. The BE and KE values were obtained by using the Peak-fit Program implemented in the control software of the spectrometer.

Gas pressure infiltration

Compacts for infiltration were prepared as described in Ref. [9]. At least 10 compacts were used to derive the average particle volume fraction V_p shown in Table 2. Gas pressure infiltration of molten Al into the TiB_2 particle compacts was carried out in a pressurized chamber at 700 ± 5 °C. Details concerning the equipment and the infiltration procedures can be found in Ref. [9].

Measurement of the intrinsic permeability of the preforms

In order to evaluate the intrinsic permeability, pressureless infiltration of an organic fluid into the compacts made of the two kinds of TiB_2 particles, was carried out at room temperature. The organic fluid used in the present study was polyethylenglycol-200 (purity of 99 wt%, hereafter referred to as PEG200). The organic fluid was dropped into the compact tube and infiltration was initiated. Infiltration height versus time was then recorded on at least three compacts that were infiltrated for each kind of particle.

Results and discussion

Characteristics of the compacts

The volume fraction attained in the compacts made out of the two types of TiB_2 particles was as high as 0.63 (Table 2), which indicates not only a proper compaction procedure but also allows inferring that the particle size distribution might be different from a purely monomodal. In fact, the reported volume fraction in compacts of identical spheres is 0.59–0.64 [10]. That the compacts of TiB_2 can be compacted up to this high degree may be a consequence of their large span (1.62 and 1.77 for TiB_2-S and TiB_2-C, respectively, as reported in Table 2), which is twice as much as that measured for regular angular particles (typically about 0.5–0.6 [5, 9]). The particle size distribution corresponding to these values of span is quite complex; the micrographs of Fig. 1 illustrate how inhomogeneous these particles are in what concerns both size and shape. Besides, the ratio of the specific surface areas determined by laser scattering $S_L = 6/(\rho D(3,2))$, ρ being

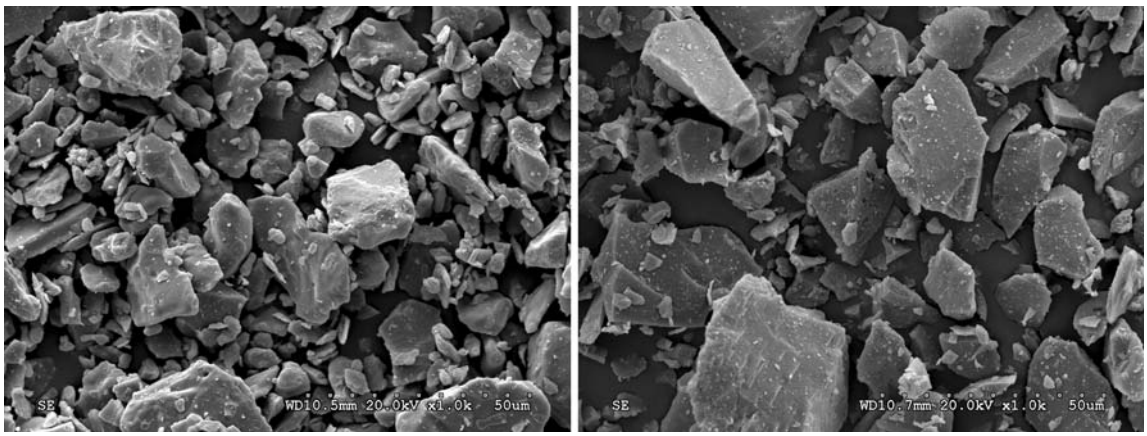

Fig. 1 SEM morphologies of the two kinds of TiB_2 particles used in the present study

the TiB_2 density (4520 kg/m^3) and by BET (both reported in Table 2), namely, $r = S_{BET}/S_L$, is 2.82 and 2.2 for the smaller and coarser particles, respectively. These values are substantially smaller than the one reported in Ref. [11], namely 4.54, that was derived from a fitting of S_{BET} versus S_L for nine kinds of SiC particles. Again, this significant difference should be a consequence of particle shape and of the significantly larger span of the TiB_2 particles investigated here.

Threshold pressures and contact angles

Infiltration data for the square of the infiltrated height have been plotted versus the applied pressure (see Fig. 2). The plots are linear fittings along the whole range of pressures whose abscissa origin gives the threshold pressure P_0. The threshold pressure for TiB_2-C compacts is only 4% larger than that for TiB_2-S, while its average particle diameter is a factor of 1.5 larger. The reason for this apparently odd behavior is the identical BET specific surface areas that these two particles have. This is an outstanding example of the predominant role of surface area over size. In order to derive contact angles from threshold pressure data we make use of the well-known "capillary law" rewritten in the form,

$$\cos\theta = \frac{P_0(1 - V_p)}{\rho\gamma_{lv}S_pV_p} \quad (1)$$

θ being the contact angle between metal and reinforcement, γ_{lv} the surface tension of the metal (around 860 mN/m for pure aluminum at 700 °C, see Ref. [12]), and V_p, ρ, and S_p denote the volume fraction, density, and specific surface area of the particulate reinforcement (actual values reported in Tables 2 and 3).

The contact angles derived from the infiltration of the two types of TiB_2 particles, namely 132° and 135° for TiB_2-C and TiB_2-S, respectively, are very close and must be understood as equivalent in terms of the wetting nature at the interface. Both values are high, indicating a non-wettable character of the metal over the surface of TiB_2 particles. Such high values of contact angle may be a consequence of: (i) the metal is oxidized and a hardly deformable oxide coating covers its surface, and/or, (ii) an

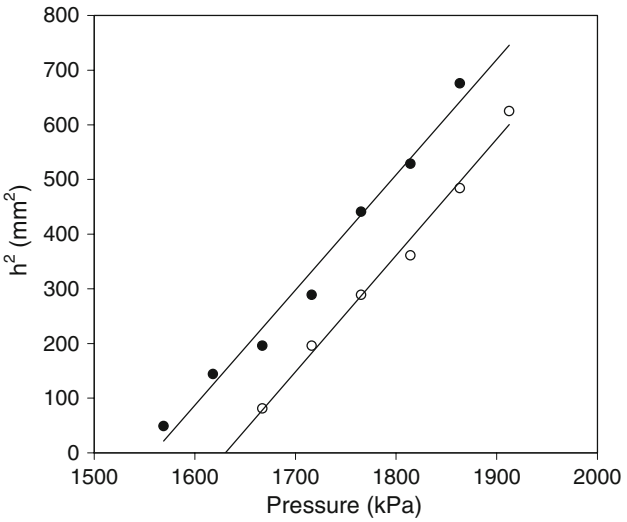

Fig. 2 Square of the infiltrated height h^2 as function of the applied pressure P for molten Al infiltrated into the compacts made of the two kinds of TiB_2 particles (*filled symbols* TiB_2-C, *open symbols* TiB_2-S). The linear fittings of the experimental data are $h^2 = 2.13(P\text{-}1630)$ mm^2 ($R = 0.995$) for TiB_2-S and $h^2 = 2.11(P\text{-}1560)$ mm^2 ($R = 0.991$) for TiB_2-C

Table 3 Derived slope S (in mm^2/kPa), permeability k (10^{-14} m^2), intrinsic permeability k_I (10^{-14} m^2), threshold pressure P_0 (kPa), and contact angle θ (°) for molten Al infiltrated into the compacts made of the two kinds of two TiB_2 particles (small S and coarse C)

System	S	k	k_I	P_0	θ
TiB_2(S)/Al	2.13	0.328	0.741	1630	135
TiB_2(C)/Al	2.11	0.325	0.705	1560	132

oxide layer covering the particles that avoids direct contact between metal and ceramic phase. We shall comment both possibilities in detail.

The infiltration experiments are carried out in air atmosphere, so the surrounding gas near the triple line is rich in oxygen and presumably the molten metal surface can be heavily oxidized during its movement along the channels of the preform. However, in previous works [13, 14] the authors have obtained experimental evidence that indicates that the metal seems to be free of any continuous oxygen layer covering its surface when it penetrates into the preform. Seemingly, forced movement of the triple line through the capillary channels of the solid preform skims off the oxide from the metallic surface [13–15]. In addition it is likely that the infiltration kinetics is too fast to allow the growth of a compact oxide layer on the melt surface. Clearly, the values derived here for contact angles must be compared with those derived from sessile drop experiments for clean metal on TiB_2 surfaces at low contact times, given the fast kinetics of pressure-driven infiltration. The fact that the contact angle is high is then a matter of the non-wetting character of the Al/TiB_2 system. Sessile drop experiments under high-vacuum conditions for the Al/TiB_2 system indicates that the contact angle steadily decreases from an initial value of roughly 140° to a very low wetting angle that, depending on several factors, including reaction time, temperature, and the nature and characteristics of the TiB_2 substrate, may reach 30° [16–18]. Three wetting stages may be distinguished during this transition from high to low contact angles in the Al/TiB_2 system:

(i) High values of contact angle near 150°, that may be attributed to the metallic de-oxidation process that takes place prior to the triple line capillary-driven movement.

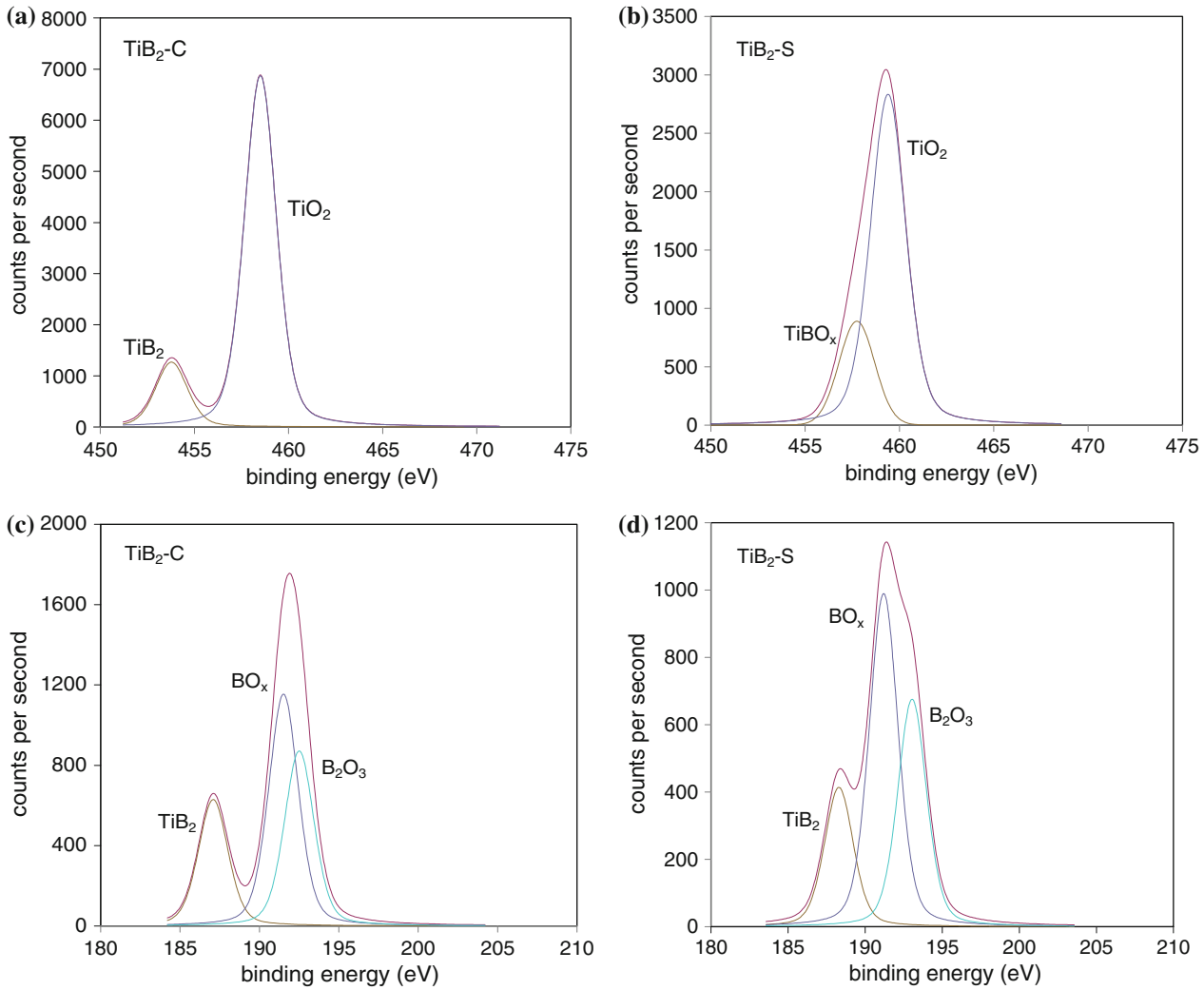

Fig. 3 X-ray photoelectron spectroscopy (XPS) spectra of the TiB_2 particles. The peaks have been assigned based on the information extracted from Refs. [20–23]

(ii) Intermediate values in the range 140°–160°, corresponding to the first kinetics of metal spreading on a naturally formed oxide layer covering the TiB_2 particle surfaces.

(iii) The final stage corresponds to the metal spreading over a free-oxygen surface of TiB_2. The final contact angle is reached after long time, 1–10 h. No reactivity at the micron scale has been found at the Al/TiB_2 interface even at temperatures higher than 750 °C.

The fact that the contact angles derived from infiltration experiments coincide with sessile drop data for the second stage of wetting, indicates that the contact during infiltration must be established between a metal surface free of a continuous oxide layer and a TiB_2 substrate that is covered by a natural oxide layer. In order to obtain chemical information about the composition of the TiB_2 particles surface, XPS measurements were carried out. Results shown in Fig. 3 illustrate the presence of different Ti oxides on the surfaces of both types of TiB_2. Given the fact that both contact angles of Al on TiB_2 are similar in spite of the different chemical oxygen content of the different TiB_2 particles, the interactions between metal and the different oxides on TiB_2 are essentially equal.

Infiltration kinetics

Figure 2 is also indicative of the kinetics of infiltration. Plots of the square of the infiltrated height (h^2) versus applied pressure (P) are linear in accordance with Darcy's law:

$$h^2 = \frac{2kt}{\mu(1 - V_p)}(P - P_o) \quad (2)$$

where k is the compact permeability, t the infiltration time (120 s in the present experiments), and μ is the viscosity of the fluid (around 1×10^{-3} Pa s for Al at 700 °C, see Ref. [19]). From the slope of the linear fittings in Fig. 2 the permeabilities of the compacts may be calculated (the two values are actually very close, see Table 3). Intrinsic permeabilities were derived from infiltration of saturating wetting liquids following a similar procedure (plotting, in this case, the square of the infiltrated height versus infiltration time). In the present case PEG200 was used as infiltrating liquid (surface tension: 42.5 mN/m; viscosity: 60×10^{-3} Pa s and a contact angle on TiB_2 of 15°). Intrinsic permeabilities are then derived from the slopes of the straight lines fitted to the experimental results (see Fig. 4; Table 3). The fact that the two intrinsic permeabilities are so close should be again a consequence of the similar shape and the almost identical specific surface area of both types of particulates [7, 11].

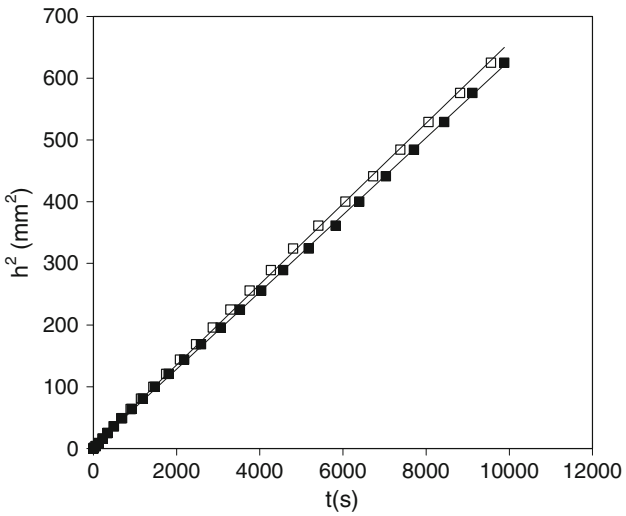

Fig. 4 Plots of the square of the infiltrated height h^2 as a function of the infiltration time t for PEG200 pressureless infiltrated into the compacts made of the two kinds of TiB_2 particles at room temperature in air (*filled symbols* TiB_2-C, *open symbols* TiB_2-S). The linear fittings of the experimental data are $h^2 = 0.0653 \times t + 4.8379$ mm^2 ($R = 0.9997$) for TiB_2-S and $h^2 = 0.0624 \times t + 3.7723$ mm^2 ($R = 0.9998$) for TiB_2-C

Concluding remarks

The following conclusions are derived from the results presented here: (i) the very similar threshold pressures and the almost identical intrinsic permeability of compacts made out of the two particles investigated here is a consequence of the very similar specific surface areas that the two particles have; (ii) the fact that the contact angles derived from infiltration experiments coincide with those measured in sessile drop experiments for the second stage of wetting indicates that contact during infiltration must be established between a metal surface free of oxides and a TiB_2 substrate that is covered by a natural oxide layer.

Acknowledgements The authors acknowledge partial financial support from: "Ministerio de Educación y Cultura" (Grant MAT2009-03139). J. M. Molina gratefully acknowledges financial support from the "Generalitat Valenciana" (project GVPRE/2008/244) and the Universidad de Alicante (project GRE08-P13). J. M. Molina also acknowledges the Spanish Ministerio de Educación y Cultura for his current "Ramón y Cajal" (formerly "Juan de la Cierva") contract.

References

1. Basu B, Raju GB, Suri AK (2006) Int Mater Rev 51:352
2. Munro RG (2000) J Res Natl Inst Stand Technol 105:709
3. Gordon FH, Turner SP, Taylor R, Clyne TW (1994) Composites 25:583
4. Subramanian C, Murthy TSRCh, Suri AK (2007) Refract Metals Hard Mater 25:345

5. Garcia-Cordovilla C, Louis E, Narciso J (1999) Acta Mater 47:4461
6. Molina JM, Piñero E, Narciso J, García-Cordovilla C, Louis E (2005) Curr Opin Solid State Mater Sci 9:202
7. Piñero E, Molina JM, Narciso J, Garcia-Cordovilla C, Louis E (2008) J Compos Mater 42:2795
8. Molina JM, Saravanan RA, Arpón R, García-Cordovilla C, Louis E, Narciso J (2002) Acta Mater 50:247
9. Alonso A, Pamies A, Narciso J, Garcia-Cordovilla C, Louis E (1993) Metall Trans A 24:1423
10. Spaepen F (1975) Acta Metall 23:729
11. Molina JM, Arpón R, Saravanan RA, García-Cordovilla C, Louis E, Narciso J (2004) Scripta Mater 51:623
12. Goicoechea J, García-Cordovilla C, Louis E, Pamies A (1992) J Mater Sci 27:5247. doi:10.1007/BF02403824
13. Molina JM, Rodríguez-Guerrero A, Bahraini M, Weber L, Narciso J, Rodríguez–Reinoso F, Louis E, Mortensen A (2007) Scripta Mater 56:991
14. Molina JM, Tian J, Garcia-Cordovilla C, Louis E, Narciso J (2007) J Mater Res 22:2273
15. Mortensen A, Wong T (1990) Metall Trans A 21:2257
16. Eustathopoulos N, Nicholas MG, Drevet B (1999) Wettability at high temperatures. Pergamon Press, Oxford
17. Passerone A, Muolo ML, Passerone D (2006) J Mater Sci 41:5088. doi:10.1007/s10853-006-0442-8
18. Weirauch DA, Krafick WJ, Ackart G, Ownby PD (2005) J Mater Sci 40:2301. doi:10.1007/s10853-005-1949-0
19. Gale WF, Totemeier TC (eds) (2004) Smithells metals reference book, 8th edn. Elsevier-ASM International, Oxford
20. Gupper A, Fernández A, Fernadez-Ramos C, Hofer F, Mitterer, Warbichler P (2002) Monatshefe für Chemie 133:837
21. Ong CW, Huang H, Zheng B, Kwok RWM, Hui YY, Lau WM (2004) J Appl Phys 95:3527
22. Chu K, Lu YH, Shen YG (2008) Thin Solid Films 516:5313
23. Zhang F, Wolf GK, Wang X, Liu X (2001) Surf Coat Technol 148:65